J Fluoresc (2009) 19:449–462
DOI 10.1007/s10895-008-0432-0

ORIGINAL PAPER

# Fluorescence, Induced Circular Dichroism and Molecular Mechanics of 1-Methyl Naphthalenecarboxylate Complexes with 2-Hydroxypropyl Cyclodextrins

**María José González-Álvarez · Antonio Di Marino · Francisco Mendicuti**

Received: 11 July 2008 / Accepted: 14 October 2008 / Published online: 7 December 2008


**Abstract** Steady-state, time-resolved fluorescence, Circular Dichroism and Molecular Mechanics techniques were used to study the complexation of 1-methyl naphthalenecarboxylate (1MN) with the 2-hydroxylpropyl-α-, -β- and -γcyclodextrins (*HP*CDs). The emission spectrum of 1MN shows two bands whose intensity ratios (*R*) are sensitive to complexation. The stoichiometry, binding constants and thermodynamics parameters upon complexation were obtained from the variation of fluorescence intensity, *R,* and lifetime averages, $\langle\tau\rangle$, with [*HP*CD] and temperature. They were then compared with the ones obtained for the complexation of 1MN with the non-substituted α-, β- and γCDs. Like the 1MN:CD complexes, the 1MN:*HP*CD ones showed 1:1 stoichiometries, but they resulted relatively more stable. Molecular Mechanics calculations in the presence of water allowed us to understand the structure of the complexes and the possible driving forces responsible for the complexation. Geometry agrees with the experimental stoichiometry and the signs of enthalpy and entropy changes. *R* for the complexes, quenching, fluorescence depolarization measurements and induced circular dichroism spectra also supported the proposed structures.

**Keywords** Cyclodextrins · Fluorescence · Circular dichroism · Molecular mechanics · 1-methyl naphthalenecarboxylate · 1-methylnaphthoate · 2-hydroxypropyl cyclodextrin

M. J. González-Álvarez · A. Di Marino · F. Mendicuti (✉)
Departamento de Química Física, Universidad de Alcalá,
28871 Alcalá de Henares, Madrid, Spain
e-mail: francisco.mendicuti@uah.es

## Introduction

Cyclodextrins (CDs) are hollow structures formed by (α-1,4)-linked α-D-glucopyranose units which have a relatively non-polar cavity. CDs are capable of forming inclusion complexes with relatively small molecule guests or even polymers [1–4]. Non-covalently bonded guest (G) to CD binding processes are reversible in solution. Chemical substitution of any of the hydroxyl groups of their glucopyranose units modifies the thermodynamics of the G/CD formation and thus many of their properties and applications [1, 2]. The microviscosity and polarity of the medium surrounding G when it penetrates into the CD cavity changes with respect to the free G in water, modifying the spectroscopic properties of chromophore-containing Gs. Among the different spectroscopies, the fluorescence techniques are some of the most used. Stoichiometries and binding constants of the complexes (*K*), $\Delta H^0$ and $\Delta S^0$ accompanying the processes as well as information about the structure of the complexes formed could be obtained from the change of the fluorescence emission intensity [5–13], the excimer formation [14–18], the fluorescence anisotropy [12, 19–22], the relative intensity of some bands of the emission spectra, [20–29] the fluorescence decay [5, 8, 9, 12, 13, 21, 22, 27–31], the energy transfer [32–34] and the fluorescence quenching [11–13, 20, 21, 28–30, 35] upon inclusion. These experimental aspects together with Molecular Modeling [36] (Molecular Mechanics [10, 20, 27–30, 37–43] and/or Molecular Dynamics [41–49]) also contribute to clarifying the complexation mechanism and driving forces involved in such processes.

Achiral chromophoric Gs may exhibit induced circular dichroism (*ICD*) upon inclusion into the CD cavity [50]. *ICD* was used to determine the stability constants and stoichiometry for G:CD complexes. However, this technique

also provides information about the complex geometry, as the sign and strength of the *ICD* signal is related to the location of the G and its interaction with the CD host [51].

We recently reported on the complexation of 1-methyl naphthalenecarboxylate (1MN) with the three naturally occurring CDs [29]. Steady-state and time-resolved fluorescence techniques and Molecular Mechanics calculations were employed for this study. Emission spectra for 1MN in the presence or in the absence of CDs exhibited two typical electronic emission bands whose intensity ratio $R$ was sensitive to medium polarity. The analysis of the variation of $R$ with [CD] and temperature revealed identical (1:1) stoichiometry for any of the CD complexes at any temperature. The formation constants at 25 °C were around 40, 360 and 110 $M^{-1}$ for 1MN complexes with α-, β- and γCDs. They were smaller than the ones forthe less bulky 2-methyl naphthalenecarboxylate (2MN) [20, 25]. Linear van't Hoff plots reveal $\Delta H^0 < 0$ but they are also smaller than those obtained for 2MN [20]. The entropy changes exhibit $\Delta S^0 < 0$ for 1MN:αCD and 1MN:βCD and $\Delta S^0 > 0$ for 1MN:γCD. In fact, in the latter case the process is entropically governed. Molecular Mechanics (MM) [29] indicates that 1MN completely penetrates into the γCD cavities, but only slightly penetrates into the cavity of the αCD. In agreement with entropy changes and the polarity surrounding 1MN estimated from $R$ at [CD]→∞, 1MN may also partially penetrate inside the βCD. Nevertheless, MM and other experimental parameters could also point towards a deeper penetration by the primary βCD face. The van der Waals non-bonded host-guest interactions were the main forces responsible for complexation. Both the possible structures and the driving forces for the formation of the complexes could justify the values and signs of $\Delta H^0$ and $\Delta S^0$.

In this paper a combination of fluorescence polarization, quenching, lifetimes and *ICD* measurements as well as MM calculations were employed to study the complexation of 1MN with 2-hydroxyl-α-, -β- and γcyclodextrins (*HP*CDs). Stoichiometries, binding constants and the thermodynamics parameters upon complexation were obtained. Experimental and theoretical data analysis was also used to interpret the changes of enthalpy and entropy upon complexation, which are related to the geometry and the driving forces responsible for the formation of such complexes. Results were compared with those obtained for 1MN with CDs and 2MN with *HP*CDs.

## Materials and methods

### Reagents and solutions

Molar substitutions for all three α-, β- and γ*HP*CDs (Aldrich) were 0.6 and the molecular weights ~1.180, ~1.400 and ~1.580 respectively. Karl-Fisher analysis reveals a 7.0, 7.1 and 6.6% water content by mass for α-, β- and γ*HP*CD respectively. 1MN was synthesized as described elsewhere [52]. 1MN/CD water solutions (milli-Q) were prepared by weight in their own quartz cells from a 1MN filtered (Millipore, cellulose 0.45 μm ∅) saturated ([1MN] ≈ $10^{-5}$–$10^{-6}$ M, constant in all experiments) aqueous solution. The content of the cells was stirred for 48 h before measuring. The α-, β- and γ*HP*CD concentrations ranged from 0 through 13.6, 10.1 and 21.7 mM respectively. Diacetyl, $(CH_3CO)_2$ (Aldrich, 98%) was used as the fluorescence quencher.

### Apparatus

Steady-state fluorescence and time-resolved measurements were performed in a SLM 8100 AMINCO and a TCSPC FL900 Edinburgh Instruments spectrofluorometers. Characteristics and measurement conditions were described previously [22]. The thyratron-gated lamp was filled with $H_2$. Data acquisition was carried out by using 1,024 channels with a time window width of 200 ns and a total of 10,000 counts at the maximum. All measurements were performed in the temperature range from 5 to 45 °C at 10 °C intervals (Huber Ministat and Techne TE-8A). Decay intensity profiles were fitted to a sum of exponential decay functions by the iterative reconvolution method [53]. Right angle geometry and square cross section quartz 10 mm path cells were used.

Induced Circular Dichroism (*ICD*) spectra were obtained by using a JASCO J-715 spectropolarimeter. Recorded spectra were the average of two scans taken at the speed of 10 nm/min with a time response of 8 s. Bandwidths were set at 2 nm and the sensitivity and resolution at 20 mdeg and 0.5 nm respectively. Measurements were performed at 25 °C in 10 mm optical path cells.

### Fluorescence methods

The average lifetime of a multiple-exponential decay function was then defined as

$$\langle \tau \rangle = \frac{\sum_{i=1}^{n} A_i \tau_i^2}{\sum_{i=1}^{n} A_i \tau_i} \quad (1)$$

where $A_i$ is the pre-exponential factor of the component with a lifetime $\tau_i$ of the multi-exponential function intensity decay.

The fractional contribution $f_i$ of each component to the steady-state intensity at the wavelength of observation, is given by [54]

$$f_i = \frac{A_i\tau_i}{\sum_{i=1} A_i\tau_i} = \frac{I_i}{\sum_{i=1} I_i} \quad (2)$$

From a dilute solution of a pair of emitting species, *i.e.* free and complexed G, assuming that they do not interact during the excited-state lifetime, <τ> is

$$\langle\tau\rangle = f_1\tau_1 + f_2\tau_2 \quad (3)$$

The fluorescence anisotropy $r$ is defined as [55]:

$$r = (I_{VV} - G\,I_{VH})/(I_{VV} + 2\,G\,I_{VH}) \quad (4)$$

where $I_{xy}$ is the intensity of the emission that is measured when the excitation polarizer is in position x (V for vertical, H for horizontal), the emission polarizer is in position y, and the $G$ factor (= $I_{HV}/I_{HH}$) corrects for any depolarization produced by the optical system.

For these kinds of systems and using the quenching-sphere-action model [56] the Stern-Volmer equations of fluorescence intensity (𝔽, measured as the area under the emission spectrum) or $\langle\tau\rangle$ can be written as,

$$\frac{\langle\tau\rangle}{\langle\tau\rangle_{q=0}} = \frac{t_f}{(1 + K_{SV,f}[Q])} + \frac{t_c}{(1 + K_{SV,c}[Q])} \quad (5)$$

and

$$\frac{\mathbb{F}}{\mathbb{F}_{q=0}} = \frac{f_f}{\{1 + K_{SV,f}[Q]\}\exp(V_f N[Q]/1000)} + \frac{f_c}{\{1 + K_{SV,c}[Q]\}\exp(V_c N[Q]/1000)} \quad (6)$$

where the $t_f$ and $t_c$ fractions are the contributions to $\langle\tau\rangle_{q=o}$ due to the free and complexed guest in the absence of the quencher; $f_f$ and $f_c$ are the fraction of total fluorescence, $\langle\tau\rangle_{q=o}$ due to both species. $K_{SV,f}$, $V_f$, $K_{SV,c}$ and $V_c$ are the Stern-Volmer constants and volume of the sphere action for the free guest and complex. These parameters were obtained for each system as described elsewhere [29, 57].

## Binding constants from fluorescence measurements

For a 1:$n$ guest:host complex (G:*HP*CD$_n$), whose global equilibrium can be written as

$$1MN + n\,HPCD \rightleftharpoons 1MN : HPCD_n \quad (7)$$

by assuming two fluorescent species, the free and the complexed G, at the equilibrium, the binding constants can be determined from the non-linear dependence of several parameters derived from fluorescence steady-state or time-resolved fluorescence techniques with [*HP*CD] according to the following expressions:

$$\text{(a)} \quad \frac{\mathbb{F}}{\mathbb{F}_0} = \frac{1 + (\mathbb{F}_\infty/\mathbb{F}_0)K[HPCD]_0^n}{1 + K[HPCD]_0^n} \quad (8)$$

where 𝔽 represents the fluorescence intensity (𝔽). Subscripts ∞ and 0 correspond to the 𝔽 values for [*HP*CD]=0 and extrapolated at [*HP*CD]→∞.

$$\text{(b)} \quad R = \frac{R_0 + R_\infty \Phi K[HPCD]_0^n}{1 + \Phi K[HPCD]_0^n} \quad (9)$$

where $R$ is the ratio of intensities of two electronic bands $R=I_{\lambda_2}/I_{\lambda_1}$, by assuming that the emission spectra show bands centered at $\lambda_1$ and $\lambda_2$. The parameter $\Phi = I_{\infty,\lambda_1}/I_{0,\lambda_1}$ can be estimated from the I($\lambda_1$) values at [*HP*CD]=0 and extrapolated at [*HP*CD]→∞. $R_\infty$ and $R_0$ are for the free and complexed G [29, 57].

$$\text{(c)} \quad \langle\tau\rangle = \frac{\tau_0 + \tau_\infty \Phi K[HPCD]_0^n}{1 + \Phi K[HPCD]_0^n} \quad (10)$$

where $\langle\tau\rangle$ is derived from Eq. 3 and by the analysis of the fluorescence decay profiles of fluorescence intensity. $\tau_0$ and $\tau_\infty$ are the fluorescence lifetimes for the free and complexed G.

$$\text{(d)} \quad r = \frac{r_0 + r_\infty \Phi K[HPCD]_0^n}{1 + \Phi K[HPCD]_0^n} \quad (11)$$

This equation was obtained under the assumption that the total anisotropy is the sum of contributions due to uncomplexed and complexed guests. If lifetime and anisotropy data are collected at $\lambda_1$, the same parameter Φ appears in Eqs. 9, 10 and 11. If they are collected at $\lambda_2$ it is not the same. There is, however, a simple relationship between them, $\Phi(\lambda_1) = \frac{R_0}{R_\infty}\Phi(\lambda_2)$ [29, 57].

It is useful to obtain a linear equation from the non-linear Eqs. 8 to 11 as:

$$\frac{[HPCD]_0^n}{(Y_0 - Y)} = \frac{1}{K\Phi\,(Y_0 - Y_\infty)} + \frac{[HPCD]_0^n}{Y_0 - Y_\infty} \quad (12)$$

where Y represents any of the 𝔽, $R$, $\langle\tau\rangle$ or $r$ parameters.

## Molecular mechanics

The 1:1 stoichiometry complexes studied were between the 2-hydroxypropyl-α-, -β- and γcyclodextrins fully substituted at C2 of the glucopyranose unit (MS=1.0) and the 1MN guest. MM calculations were mainly performed in the presence of water by using Sybyl 6.9 from Tripos Associates, St. Louis, Missouri [58–60]. MM calculation

details and complexation procedures were identical to those reported previously [26–29].

Binding energy, $E_{binding}$ (or any non-bonded energy interaction) between 1MN and *HP*CD is obtained as the difference between the potential energy of the system and the sum of the potential energies of the isolated 1MN and *HP*CD. Strain energy is the sum of bond stretching, bond angle bending and torsion energy terms.

For complexation processes, each *HP*CD host was placed so that the center of mass of glycosidic oxygens (o) was located at the origin of a coordinate system with the y axis oriented along the main CD axis and the z axis passing trough a glycosidic oxygen. The oo' projection on the *y* coordinate (o' corresponds to the center of mass of the guest naphthalene ring), the angle between the yz and the naphthalene planes (θ) and the oo'C9 angle (δ) were used to define the relative guest-host orientation. As reported elsewhere [29] four guest-host approaching orientations named V*P*, V*nP*, H*P* and H*nP* were considered. Critical analysis of $E_{binding}$ for the structures, obtained by scanning δ, θ and *y* parameters in the vacuo, provides better orientation for the approaching. With the fixed δ and θ the guest was forced to approach *y* = 20 (Å) up to -20 (Å) at 0.5 Å steps along the *y* coordinate. Each structure generated was solvated (PBC), optimized and analyzed.

## Results and discussion

Absorption spectra for 1MN and 1MN/*HP*CD solutions in the 250–360 range show a main band centered at 294 nm and a shoulder at around 320 nm. No isosbestic points are observed upon *HP*CD addition but intensity increases. Excitation spectra in the absence of *HP*CD, as well as in presence of it, show a band centered at approximately 305 nm and a shoulder at 320 nm. Intensity decreases and slight red shifts are observed upon increasing [*HP*CD].

Figure 1 depicts the emission spectra for 1MN and 1MN/*HP*CD water solutions upon excitation of 294 nm at 25 °C. All spectra exhibit a large band placed in the 385–390 nm range and a shoulder centered at 365 nm, which are typical for the 1MN monomer emission. A decreasing in the fluorescence intensity takes place upon addition of *HP*CD, the amount of which depends on the host type and temperature. They also show isoemisive points which are placed close to the high energy shoulder: at approx. 355 nm for 1MN/α*HP*CD and at 363 nm for 1MN/β*HP*CD and 1MN/γ*HP*CD solutions. One of the main characteristics, however, is the decreasing in the intensity of the low energy band relative to the shoulder placed at ~365 nm ($R = I_{\lambda=385\ nm}/I_{\lambda=365\ nm}$) upon *HP*CD addition.

Figure 2, upper and lower panels, depicts the relative variation in fluorescence intensity ($\mathbb{F}/\mathbb{F}_0$) and the parameter

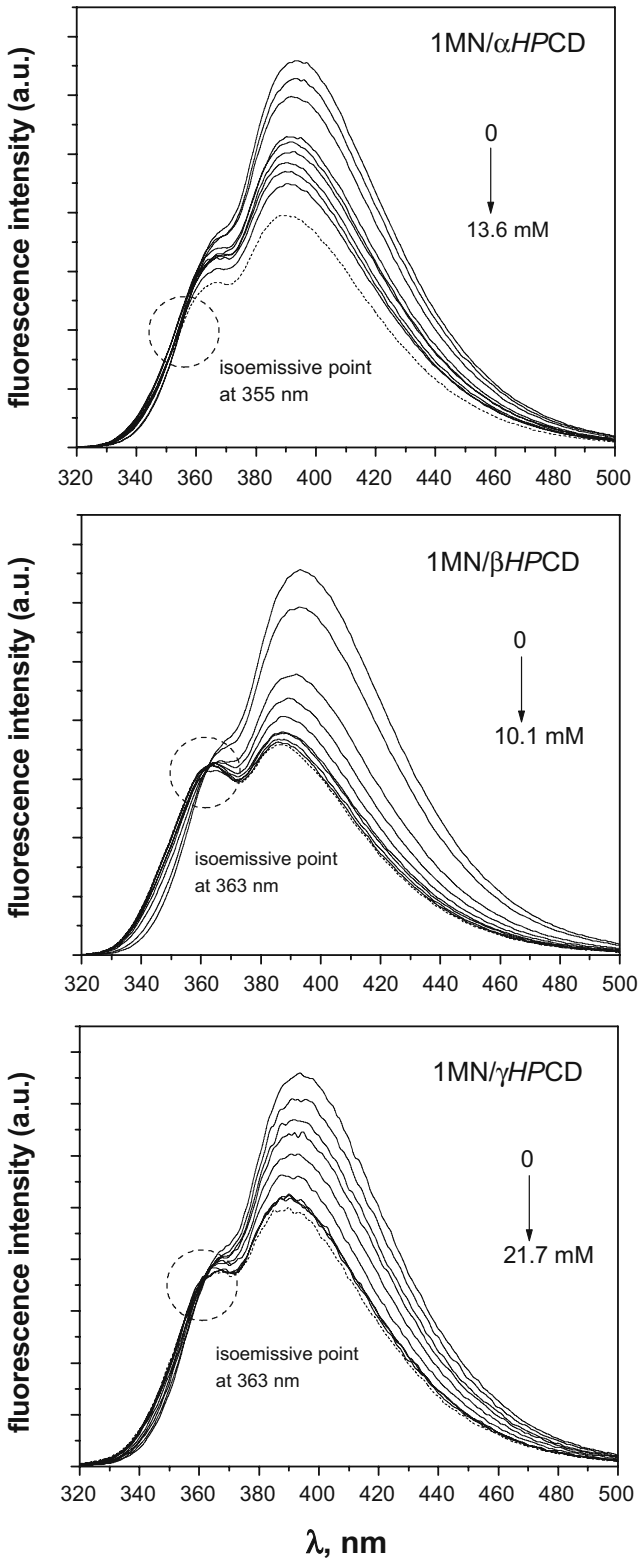


**Fig. 1** Uncorrected emission spectra of 1MN and 1MN/*HP*CD (α-, β- or γ*HP*CD) aerated water solutions at different [*HP*CD] at 25 °C upon $\lambda_{exc}$=294 nm. (*top*) [α*HP*CD] = 0, 0.56, 2.2, 3.9, 5.5, 7.1, 8.7, 10.4 and 12.2 mM; (*middle*) [β*HP*CD]= 0; 0.37, 1.5, 2.7, 4.1, 5.2, 6.6, 7.8, 8.9 and 10.1 mM. (*bottom*); [γ*HP*CD]= 0, 0.78, 2.1, 3.3, 5.5, 9.8, 14.2, 15.5, 18.4 and 21.7 mM. Notice isosbestic points

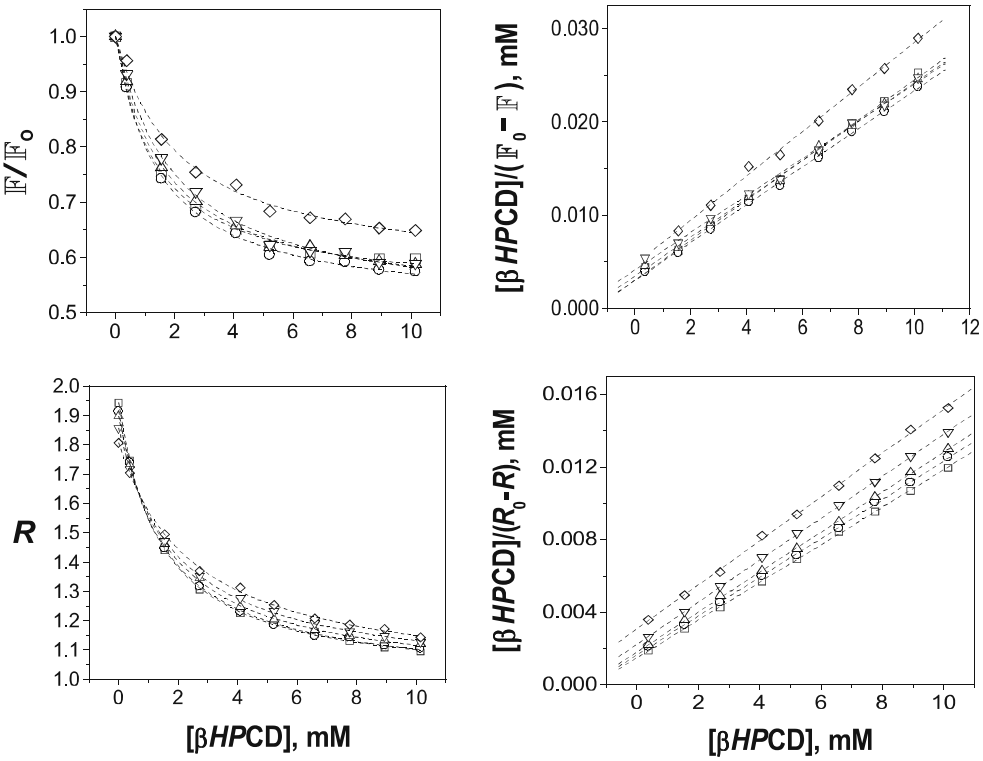


**Fig. 2** (*left*) Variation of the $\mathbb{F}/\mathbb{F}_0$ ratios and *R* parameter *vs.* [βHPCD] for 1MN/β*HP*CD water solutions at different temperatures: 5 °C (□); 15 °C (○); 25 °C (△); 35 °C (▽); and 45 °C (◊). (right) Linear representations of $\mathbb{F}$ and *R* parameters according to Eq. (12). Dashed lines were obtained by adjusting the experimental data to the proper stoichiometry by using non-linear (8) and (9) and linear (12) equations

*R* with [*HP*CD] and temperature respectively for the 1MN/β*HP*CD system. Other systems exhibit a similar, nevertheless quantitatively different, trend. The largest variation of *R* takes place for 1MN/β*HP*CD. The decreasing in *R* is associated with the decreasing in polarity of the medium surrounding the guest during complexation [29].

Fluorescence intensity decay measurements at 385 nm upon excitation of 294 nm for isolated 1MN and 1MN/*HP*CD water solutions were obtained from 5 °C to 45 °C at 10 °C intervals. The intensity profile for the isolated 1MN is mono-exponential (lifetimes from ~7.8 ns at 5 °C to ~7.2 ns at 45 °C) [29]. However, for 1MN/*HP*CD solutions these decay profiles, some of which are depicted in Fig. 3, are bi-

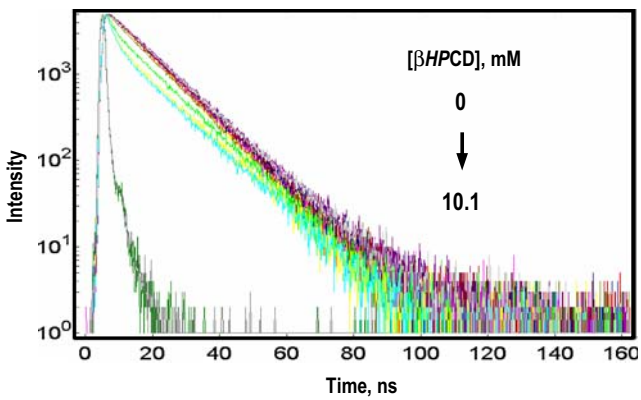


**Fig. 3** Intensity decay profiles for 1MN/β*HP*CD water solutions at different [β*HP*CD] at 25 °C upon excitation and emission wavelength of 294 and 385 nm respectively

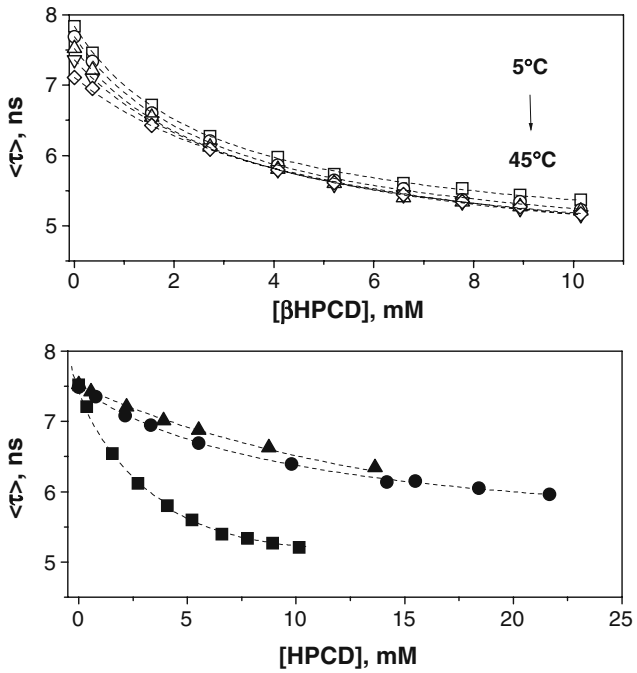


**Fig. 4** (*top*) Variation of the weighted average lifetimes, <τ> *vs.* [HPCD] for 1MN/β*HP*CD water solutions at different temperatures: 5 °C (□); 15 °C (○); 25 °C (△); 35 °C (▽); and 45 °C (◊). (*bottom*) Idem for all 1MN/*HP*CD systems: 1MN/α*HP*CD (■), 1MN/β*HP*CD (●) and 1MN/γ*HP*CD (▲) at 25 °C. *Dashed lines* were obtained by adjusting the experimental data to the proper stoichiometry by using non-linear Eqs. (10) and (11)

exponential. The fast component, whose contribution increases with [*HP*CD], is attributed to the complex. The slow one, which matches the one for the isolated 1MN very well, is attributed to the free guest.

Figure 4 depicts the decrease of $\langle\tau\rangle$ with [β*HP*CD] at different temperatures and for the three 1MN/*HP*CD systems at 25 °C. The largest decrease in <τ> with [*HP*CD] is obtained for 1MN/β*HP*CD as occurred for 1MN/βCD [29]. This decrease, which was also observed when 2MN complexes with β*HP*CD [21] and for the complexation of 1MN with natural un-modified CDs [29], is a consequence of the faster lifetime component for the complexed form as compared to the free one.

The binding constants (*K*) obtained by the non-linear (Eqs. 8–10) and linear adjustments (Eq. 11) by using different steady-state and time resolved fluorescence techniques are collected in Tables 1 and 2. Examples of these adjustments are also depicted in Fig. 2. The *K* averages at 25 °C were ~70, ~590 and ~155 $M^{-1}$ (steady-state, from $\mathbb{F}$ or *R*) and ~115, ~565 and ~145 $M^{-1}$ (from lifetime measurements) for 1MN complexed with α-, β- and γ*HP*CD respectively. Broadly speaking, they were lower when compared to the ones for the 2MN/*HP*CD [21] complexes and for 2,3-naphthalenedicarboxylate (23DMN) with the same *HP*CDs [61], but always larger than when 1MN complexes with the natural un-substituted CDs [21, 61]. The values of $\Phi(\lambda_1)$ are close to 1, *i.e.* $I_\infty(\lambda_1) \approx I_0(\lambda_1)$. $\Phi(\lambda_2)$ values stay around 0.5–0.7 (at $\lambda_2$= 385 nm $I_\infty(\lambda_2) < I_0(\lambda_2)$). They do not show any great change with temperature.

The Job's Plots [62, 63] depicted in Fig. 5 denote a 1:1 stoichiometry for all the 1MN:*HP*CD complexes.

As an example, Fig. 6 depicts linear van't Hoff plots obtained from the average of the *K* values from the steady-state measurements collected in Table 1. Table 3 shows $\Delta H^0$ and $\Delta S^0$ for 1MN:*HP*CD complexes obtained from

**Table 1** $\mathbb{F}_\infty/\mathbb{F}_0$, $R_\infty$,$\Phi(\lambda_1 = 365\ nm)$ parameters and binding constants *K*, obtained from steady-state fluorescence measurements at five temperatures for three systems studied

| | Fluorescente Intensity ($\mathbb{F}$) | | | Intensity ratios, (*R*) | | |
|---|---|---|---|---|---|---|
| | T (°C) | $\mathbb{F}_\infty/\mathbb{F}_0$ | *K* ($M^{-1}$) | $\Phi(\lambda_1)$ | $R_\infty$ | *K* ($M^{-1}$) |
| 1MN/α*HC*D | 5 | 0.30±0.05 | 106±15 | 1.00 | 1.12±0.04 | 179±21 |
| | | | **163±20** | | **1.26±0.07** | **110±21** |
| | 15 | 0.31±0.07 | 98±18 | 1.06 | 1.07±0.03 | 116±9 |
| | | | **122±8** | | **1.22±0.06** | **76±11** |
| | 25 | 0.25±0.10 | 76±18 | 1.10 | 1.04±0.06 | 78±9 |
| | | | **90±6** | | **1.26±0.09** | **61±14** |
| | 35 | 0.25±0.09 | 67±13 | 1.09 | 1.21±0.04 | 112±15 |
| | | | **99±11** | | **1.35±0.04** | **85±10** |
| | 45 | 0.05±0.13 | 33±6 | 1.09 | 1.12±0.05 | 59±7 |
| | | | **64±8** | | **1.27±0.07** | **45±8** |
| 1MN/β*HP*CD | 5 | 0.53±0.01 | 710±46 | 1.07 | 0.981±0.005 | 658±16 |
| | | | **710±65** | | **0.978±0.006** | **645±20** |
| | 15 | 0.51±0.01 | 678±36 | 1.06 | 0.976±0.006 | 607±15 |
| | | | **675±43** | | **0.978±0.005** | **611±20** |
| | 25 | 0.52±0.01 | 603±35 | 1.04 | 0.985±0.005 | 570±13 |
| | | | **593±39** | | **0.988±0.005** | **581±14** |
| | 35 | 0.50±0.01 | 492±37 | 1.01 | 0.991±0.003 | 508±7 |
| | | | **478±41** | | **0.991±0.003** | **508±9** |
| | 45 | 0.57±0.01 | 457±50 | | 0.984±0.011 | 400±16 |
| | | | **504±53** | 0.99 | **0.980±0.009** | **393±15** |
| 1MN/γ*HP*CD | 5 | 0.60±0.02 | 162±23 | 1.12 | 1.20±0.02 | 127±10 |
| | | | **148±13** | | **1.21±0.01** | **136±5** |
| | 15 | 0.56±0.02 | 116±11 | 1.06 | 1.20±0.02 | 152±11 |
| | | | **118±12** | | **1.20±0.02** | **153±12** |
| | 25 | 0.591±0.013 | 151±14 | 1.04 | 1.19±0.01 | 167±10 |
| | | | **148±13** | | **1.18±0.01** | **159±7** |
| | 35 | 0.569±0.013 | 145±12 | 1.03 | 1.16±0.03 | 145±19 |
| | | | **143±13** | | **1.17±0.01** | **151±14** |
| | 45 | 0.62±0.04 | 79±17 | 1.01 | 1.19±0.01 | 169±7 |
| | | | **74±8** | | **1.20±0.01** | **174±8** |

*K* values were obtained by using the non-linear (Eqs. 8 and 9) and (bold) the linear (Eq. 12) adjustments

**Table 2** $\langle\tau\rangle_\infty$, $\Phi(\lambda_2 = 385\ nm)$ and binding constants $K$, obtained from lifetime fluorescence measurements at five temperatures for three systems studied

| | Lifetime Average ($\langle\tau\rangle$) | | | |
|---|---|---|---|---|
| | T (°C) | $\Phi_{385}$ nm | $\langle\tau\rangle_\infty$ (ns) | $K$ ($M^{-1}$) |
| 1MN/α*HP*CD | 5 | 0.58 | 5.24±0.07 | 153±8 |
| | | | **5.1±0.2** | **135±16** |
| | 15 | 0.59 | 5.12±0.04 | 127±3 |
| | | | **5.07±0.05** | **123±3** |
| | 25 | 0.61 | 4.99±0.08 | 104±5 |
| | | | **5.24±0.17** | **123±14** |
| | 35 | 0.63 | 5.06±0.19 | 102±13 |
| | | | **5.27±0.17** | **119±15** |
| | 45 | 0.68 | 5.14±0.11 | 88±8 |
| | | | **5.20±0.15** | **92±10** |
| 1MN/β*HP*CD | 5 | 0.54 | 4.69±0.03 | 672±20 |
| | | | **4.70±0.03** | **681±19** |
| | 15 | 0.54 | 4.51±0.04 | 613±21 |
| | | | **4.52±0.03** | **620±21** |
| | 25 | 0.54 | 4.42±0.04 | 566±23 |
| | | | **4.48±0.04** | **563±22** |
| | 35 | 0.54 | 4.31±0.02 | 480±8 |
| | | | **4.30±0.02** | **563±9** |
| | 45 | 0.54 | 4.20±0.05 | 368±16 |
| | | | **4.21±0.03** | **374±11** |
| 1MN/γ*HP*CD | 5 | 0.69 | 5.84±0.07 | 157±13 |
| | | | **5.88±0.07** | **167±14** |
| | 15 | 0.66 | 5.43±0.06 | 144±8 |
| | | | **5.46±0.05** | **149±8** |
| | 25 | 0.65 | 5.24±0.05 | 151±8 |
| | | | **5.16±0.09** | **138±11** |
| | 35 | 0.65 | 4.88±0.11 | 128±12 |
| | | | **4.95±0.10** | **138±12** |
| | 45 | 0.66 | 4.95±0.03 | 147±5 |
| | | | **4.91±0.04** | **140±6** |

*K* values were obtained by using the non-linear (Eq. 10) and (bold) the linear (Eq. 12) adjustments.

steady-state and lifetime measurements. This table also shows the thermodynamics parameters for 2MN:*HP*CD [21] and 1MN:CD [29] complexes that were obtained from steady-state measurements. $\Delta H^0$ and $\Delta S^0$ for 1MN:*HP*CD complexes exhibit values obtained from steady-state and time-resolved (less reliable due to intrinsic reasons) measurements which are within the standard deviation. The exception, as with 1MN/αCD, is for the 1MN complex with the smallest size *HP*CD.

Complexations of 1MN with α- and β*HP*CD have $\Delta H^0<0$. The complex with γ*HP*CD, however, shows $\Delta H^0\approx 0$. As with most of the cases [20, 21, 35, 43], the decreasing in the CD macro-ring size means a more favorable $\Delta H^0$. Complexation processes of 1MN with *HP*CDs are also accompanied by less favorable enthalpy changes than the ones obtained with their natural counterparts [29]. Something similar occurred when 2MN was complexed with *HP*CDs

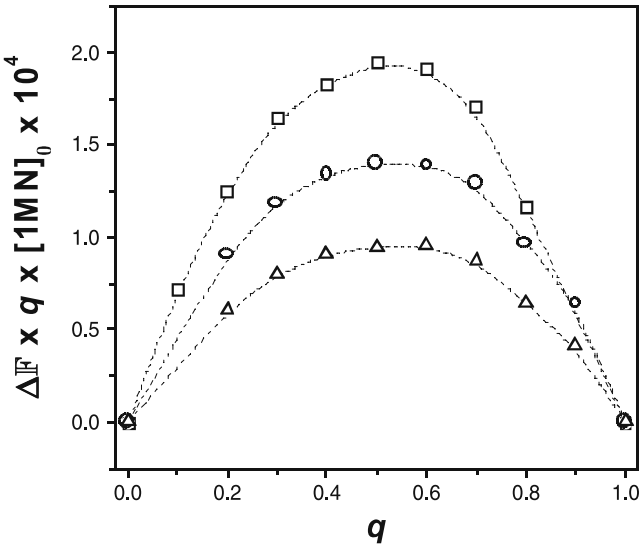


**Fig. 5** Job's plots for the 1MN/α*HP*CD (□), 1MN/β*HP*CD (○) and 1MN/γ*HP*CD (△) systems. $\Delta\mathbb{F}=\mathbb{F}_0-\mathbb{F}$ is the difference of fluorescence intensity in the absence and in the presence of *HP*CD and $q$ is defined as $[HPCD]_t/\left([G]_t+[HPCD]_t\right)$, where $[HPCD]_t$ and $[G]_t$ are the *HP*CD CD and G concentrations

[21]. The increase in the cavity size (width and/or length) [20, 21, 25, 43] generally makes van der Waals attractive interactions decrease, and $\Delta H^0$ is then less favorable or slightly unfavorable. Thus $\Delta H^0$ values and trends would agree with the possibility that van der Waals attractive interactions may be responsible for the formation of 1MN/*HP*CD complexes.

When comparing the results from steady-state measurements, $\Delta S^0$ signs upon 1MN/*HP*CDs formation match those obtained for 2MN/*HP*CD systems [21] and partially the ones obtained for complexation of 1MN with their natural counterparts [29]. $\Delta S^0<0$ if 1MN complexes with

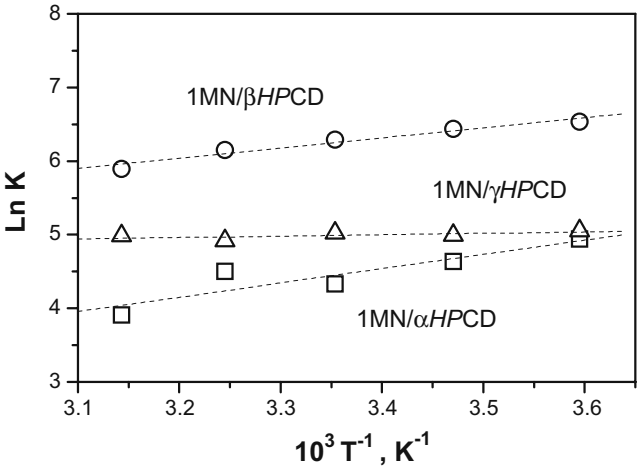


**Fig. 6** Van't Hoff plots of RLn $K$ *vs.* $T^{-1}$ for the formation of 1MN complexes with α *HP*CD (□), β*HP*CD (○) and γ*HP*CD (△) from the average of binding constants obtained by $\mathbb{F}$ and $R$ steady-state measurements

**Table 3** Values of the enthalpy ($\Delta H^0$) and entropy ($\Delta S^0$) changes associated to the complexation processes of 1MN with α-, β- and γ*HP*CDs from the average of the values of *K* obtained by steady-state (ss) and time-resolved (tr) fluorescence measurements

| complex | $\Delta H^0_{ss}$ (kJmol$^{-1}$) | $\Delta S^0_{ss}$ (JK$^{-1}$mol$^{-1}$) | $\Delta H^0_{tr}$ (kJmol$^{-1}$) | $\Delta S^0_{tr}$(JK$^{-1}$mol$^{-1}$) |
|---|---|---|---|---|
| **1MN:α*HP*CD** | **−16±4** | **−17±14** | **−7±2** | **+17±7** |
| 2MN:α*HP*CD | −25±1 | −28±4 | | |
| 1MN:αCD | −15±7 | −21±25 | | |
| **1MN:β*HP*CD** | **−7±2** | **+30±7** | **−10±1** | **+17±4** |
| 2MN:β*HP*CD | −8±3 | (+40±7) | | |
| 1MN:βCD | −18±5 | −15±11 | | |
| **1MN:γ*HP*CD** | **+0±1** | **+42±4** | **−1±1** | **+38±2** |
| 2MN:γ*HP*CD | +6±3 | +63±11 | | |
| 1MN:γCD | −3±2 | +25±7 | | |

Are also enclosed the values for 2MN:α*HP*CD [21] and 1MN/CD [29]

α*HP*CD and $\Delta S^0>0$ when it does with β- and γ*HP*CD. The entropic terms accompanying the complexation are more favorable (β- and γ*HP*CDs) or less unfavorable (α*HP*CDs) than with their natural counterparts. Something similar was reported when comparing $\Delta S^0$ for 2MN complexation with *HP*CD and CDs [21]. The entropy sign upon complexation is usually the result of two opposite terms: a positive one, which corresponds to the loss of the ordered water surrounding the guest or included inside the CD host, and a negative one due to the decrease in the degrees of freedom. In general, an increase in the macro-ring size is accompanied by a more favorable or less unfavorable entropic term. Thus $\Delta S^0<0$ for 1MN/α*HP*CD is typical of guests whose penetration into the relatively small cavity is partial and whose movement is also fairly hindered. The $\Delta S^0>0$ for 1MN with β- and γ*HP*CDs may indicate that the 1MN penetrates into the β- and γCD cavities.

The variation of the fluorescence anisotropy (*r*) with [β*HP*CD] at different temperatures is represented in the left panel of Fig. 7 for the 1MN/β*HP*CD system. The right panel shows the change in *r* for all the systems at a single temperature. The curves are the result of the adjustments of the data to Eq. (11). *r* increases with [*HP*CD] and it decreases with temperature. This can be attributed to the larger fraction of 1MN complexed and to the decrease in the viscosity solvent and/or to the decreases in the complexed fraction as the processes are enthalpically favored. $r_\infty$ for the complexed forms varies as: $r_{\infty,1MN:\alpha HPCD}(=0.039) > r_{\infty,1MN:\beta HPCD}(=0.034) > r_{\infty,1MN:\gamma HPCD}(=0.029) > r_{0,1MN}$. The largest value obtained for 1MN:α*HP*CD would be in agreement with the formation of a rigid complex, where 1MN, which is partially inside the cavity, strongly interacts with α*HP*CD. The decrease in *r* with the host size may indicate, in agreement with the $\Delta S^0$ sign, a deeper penetration of 1MN. Although the trend in *r* is different with un-substituted CDs ($r_{\infty,1MN:\gamma CD} > r_{\infty,1MN:\alpha CD} > r_{\infty,1MN:\beta CD} >> r_{0,1MN}$) similar conclusions were drawn with regard to the 1MN/αCD complex [29].

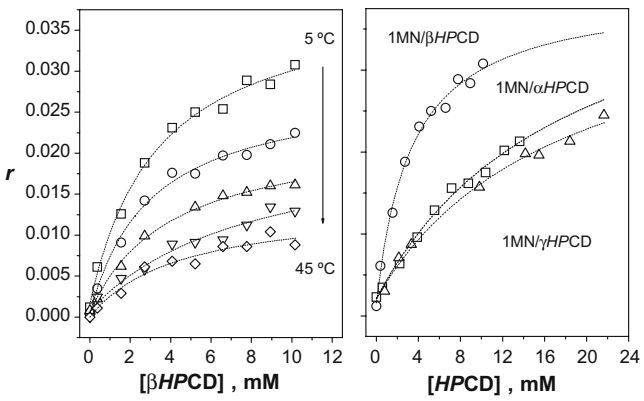


**Fig. 7** (*left*) Variation of the fluorescence anisotropy (*r*) with [β*HP*CD] and temperature (T) for the 1MN/β*HP*CD system; T=5 °C (□); 15 °C (○); 25 °C (△); 35 °C (▽); and 45 °C (◊). (*right*) Variation of *r* with [*HP*CD] for 1MN/*HP*CD systems at 5 °C: α*HP*CD (□), β*HP*CD (○) and γ*HP*CD (△). Experiments were performed at $\lambda_{ex}$=294 nm and $\lambda_{em}$=385 nm

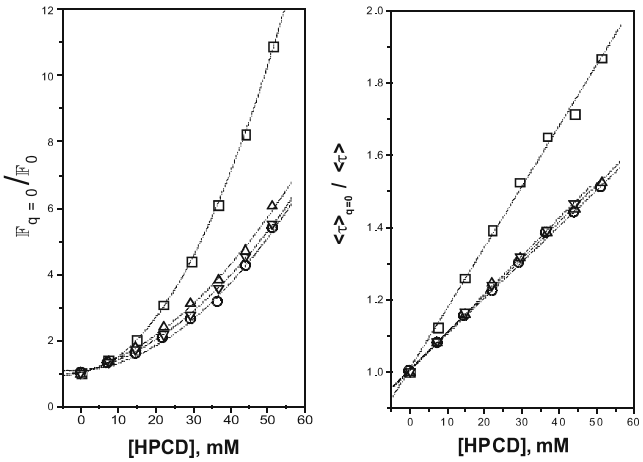


**Fig. 8** Stern-Volmer representations obtained from steady-state (*left*) and time-resolved (*right*) fluorescence measurements for 1MN (□), 1MN/α*HP*CD (○), 1MN/β*HP*CD (△) and 1MN/γ*HP*CD (▽) systems at 25 °C. Quencher was 2,3-butanedione (diacetyl)

Figure 8 depicts Stern-Volmer plots from $\langle\tau\rangle$ (right) and $\mathbb{F}$ (left) measurements on free 1MN and 1MN/*HP*CD solutions (fraction of the complexed guest fixed at 0.75 for all systems) by using diacetyl $(CH_3CO)_2$ as a quencher. Several aspects from the experiments must be pointed out: (a) $R$ hardly changes upon quencher addition; (b) $\langle\tau\rangle_{q=0}/\langle\tau\rangle$ varies linearly with [Q] with the largest $K_{SV}$ for 1MN in the absence of CD; (c) $\mathbb{F}_{q=0}/\mathbb{F}$ plots deviate from the linearity. The parameters collected in Table 4 were obtained by fitting the experimental steady-state and time-resolved data to the quenching-sphere-action model following the procedure described elsewhere [29, 56, 57]. $K_{SV,f}$ for free 1MN is 2–3 times larger than $K_{SV,c}$, following $K_{SV,1MN} > K_{SV,1MN:\alpha HPCD} > K_{SV,1MN:\gamma HPCD} > K_{SV,1MN:\beta HPCD}$. The bimolecular quenching constants ($k_{q,c}$) follow a similar trend. These results may indicate that the free 1MN is easier to access than when it is complexed, but also, in agreement with $r_\infty$ values and $\Delta S^0$ signs, that the accessibility to 1MN is slightly larger for 1MN:α*HP*CD than for the other two complexes. The comparison of the results of $K_{SV,c}$ and $k_{q,c}$ with those obtained for 1MN complexation with the unsubstituted CD partners [29] reveals a slightly better penetration of the 1MN inside *HP*CD cavities.

The dependence of the $R$ and τ parameters for 1MN on the polarity ($\varepsilon$) and microviscosity ($\eta$) were also obtained by performing steady-state and time-resolved measurements of 1MN in different $\varepsilon$ and $\eta$ solvents [29]. Emission spectra exhibited similar features as in water, even though intensity decays were generally bi-exponential [29]. $R$ increased with $\varepsilon$ according to $R = 0.68 + 1.1 \times 10^{-3} \in +1.8 \times 10^{-4} \in^2$ at 25 °C. Something similar occurred with $\langle\tau\rangle$ which increased with $\varepsilon$ for $\varepsilon$>30, but it stayed almost constant for $\varepsilon$<30. Neither $\langle\tau\rangle$ nor $R$ showed any clear dependence on $\eta$. The values of $R_\infty$ (1.15, 0.99 and 1.19) and $\tau_\infty$ (5.1, 4.5 and 5.5 ns) for α-, β- and γ*HP*CDs at 25 °C can provide information about the 1MN guest location in the complex. With $R_\infty$ and the above $R(\varepsilon)$ equation, values of $\varepsilon \approx 47\pm5$, $39\pm1$ and $49\pm1$ respectively were estimated for the medium surrounding the 1MN guest in the complexes with α-, β- and γ*HP*CDs. These values were slightly smaller than the ones obtained for the 2MN probe with the *HP*CDs ($\varepsilon \approx 51$, 44, and 56 respectively) [21]. MM calculations on the latter systems revealed that 2MN deeply penetrates into the three *HP*CDs. Then $\varepsilon$ values provided polarities for the *HP*CD inner cavities which were quite similar for the three *HP*CDs [43]. However, 1MN was located in a slightly more polar environment when it was complexed with α-, β- and γCDs ($\varepsilon \approx 57$, 59, 61 respectively). The bulkier characteristics of 1MN, as compared to 2MN, makes it somewhat more exposed to the water polar solvent when it complexes with the α- and βCDs, whose inner cavity was estimated to be less polar ($\varepsilon$ of ~10 and ~49 respectively) [20, 25].

R and τ changes with $\varepsilon$ may also explain the monotonic decrease in $R$ and $\langle\tau\rangle$ with [*HP*CD]. This may be due to the decrease in the medium polarity surrounding 1MN when it migrates from an aqueous medium ($\varepsilon \sim 78$) to one of $\varepsilon \approx$ 40–50.

Induced circular dichroism (*ICD*) was measured for the $^1L_a$ (and $^1L_b$) absorption band placed at 294 nm (320 nm) [64], whose transition moment nearly follows the direction of the short naphthalene axis [65, 66]. Figure 9 depicts *ICD* spectra at 25 °C for isolated 1MN and 1MN/*HP*CD water solutions for the $^1L_a$ naphthalene absorption band which overlaps with the $^1L_b$ one. All 1MN/*HP*CD solutions were prepared for a fraction of approximately 0.7 of the complexed guest. Figure 9 also shows the absorption spectrum for 1MN. The *ICD* spectra for any of the 1MN with α-, β- and γ*HP*CD water solutions exhibit positive bands. The spectrum is substantially more intense for 1MN/γ*HP*CD and less for 1MN/β*HP*CD. A weaker one is obtained for the 1MN/α*HP*CD water solution and the intensity is close to the background instrument noise for 1MN in the absence of *HP*CDs. The *ICD* spectrum positive sign may agree with a 1MN guest approaching the *HP*CDs (VP or V*n*P), where the short naphthalene axis (direction of the $^1L_a$ transition moment) is nearly parallel to the *n*-fold rotation *HP*CD axis. The high intensity for the 1MN/γ*HP*CD solution suggests a better fit and/or deeper penetration of 1MN inside the γ*HP*CD, whose movement could probably be quite hindered. The weak intensity for 1MN/α*HP*CD, in agreement with $k_{q,c}$, $r_\infty$ and $\Delta S^0$ values, is derived from the poor 1MN penetration into the α*HP*CD.

In addition, *ICD* spectra for 1MN with natural CDs were also performed at the same experimental conditions. Spectra for 1MN/βCD and 1MN/γCD water solutions,

**Table 4** Parameters of the modified Stern-Volmer equation for quenching of free 1MN and 1MN/HPCD complexes at 25 °C

| system | $\tau_{c,q=0}$ ($\tau_{f,q=0}$), ns | $\langle\tau\rangle_{q=0}$, ns | $K_{SV,c}$ ($K_{SV,f}$), $M^{-1}$ | $k_{q,c}\times10^{-9}$ ($k_{q,f}\times10^{-9}$), $M^{-1}$ $s^{-1}$ |
|---|---|---|---|---|
| 1MN | (7.6±0.0) | 7.6 | (16.8±0.4) | (2.2±0.1) |
| 1MN/α*HP*CD | 5.0±0.1 | 5.7 | 7.0±0.1 | 1.4±0.0 |
| 1MN/β*HP*CD | 4.4±0.0 | 5.6 | 5.4±0.1 | 1.2±0.0 |
| 1MN/γ*HP*CD | 5.2±0.1 | 6.1 | 6.7±0.1 | 1.3±0.0 |

Quencher was diacetyl, x2=0.75 and λex=294 nm

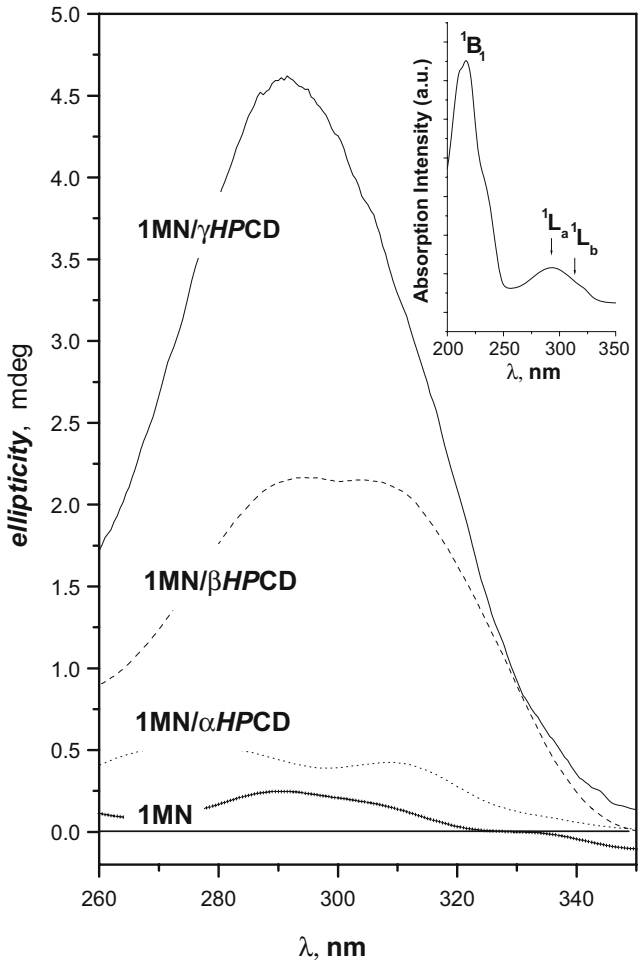


**Fig. 9** Induced circular dichroism spectra (*ICD*) at 25 °C of 1MN and 1MN/HPCD water solutions, for a [*HP*CD] which provides a 0.7 fraction of complexed guest

not shown, were also positive. As with *HP*CD solutions, the intensity was slightly larger for the latter one. The spectrum for 1MN/αCD, on the other hand, exhibited a low intensity negative band. The sign of the *ICD* when the chromophore is located mostly outside the cavity becomes opposite to that of the one inside [67–69]. Fluorescence and Molecular Mechanics results [29] for 1MN/αCD systems indicate that 1MN is predominantly outside the αCD cavity when it approaches in *V* mode and penetrates a little more when it does in the *H* one. In both cases a negative *ICD* may be expected. The fact that 1MN prefers approaching the γCD by the V*P* orientation and penetrates totally inside its cavity may agree with a large positive band. For the 1MN:βCD complex two possible V*P* structures were proposed [29]. The energetically favourable one, where 1MN penetrates almost totally inside the cavity by the primary face, would be in agreement with the positive *ICD* spectra.

Figure 10 depicts $E_{binding}$ variations obtained from the MM analysis for 1MN approaching α-, β- and γ*HP*CDs by four V*P*, V*nP*, H*P* and H*nP* orientations. As Fig. 10 shows, whatever the 1MN orientations is, the 1MN/α*HP*CD system exhibits a very high repulsive energetic barrier beginning at *y*=~5 Å, which impedes 1MN from going further along this *y* coordinate. This barrier, however, is hardly significant for 1MN/βCD and 1MN/γCD systems when 1MN approaches the *HP*CD by V*P* and V*nP* orientations. Both V*P* and V*nP* orientations yield very similar binding energies changes upon approaching and are considerably more favorable than the H*P* or H*nP* ones. Thus, 1MN may have no chance at all to totally penetrate the α*HP*CD cavity. This penetration is notably deeper, however, when β- and γ*HP*CDs are used as hosts. The fact that 1MN is totally shielded from the solvent in the latter complexes while it is not totally shielded when 1MN complexes with α*HP*CD should explain the $\Delta S^0>0$ and $\Delta S^0<0$ respectively.

In Fig. 11 some of the possible structures with minima binding energies (MBE) for 1MN/*HP*CD systems are depicted. These are reached at *y*=5.3 Å; $E_{MBE}=-41.3$ kJmol$^{-1}$ (δ=90.3°) and *y*=5.8 Å; $E_{MBE}=-34.0$ kJmol$^{-1}$ (δ=9.9°) for

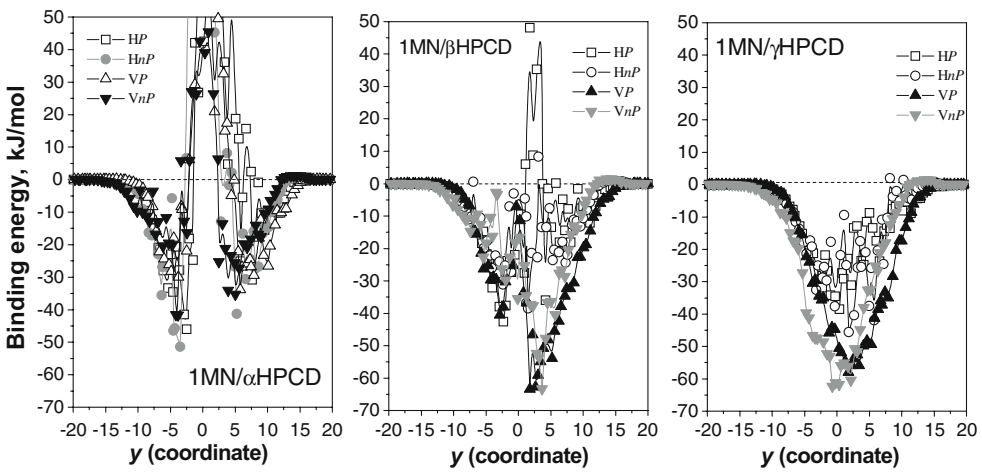


**Fig. 10** Variation of binding energy upon 1MN approaching to *HP*CD along the *y* coordinate (Å) for the three systems

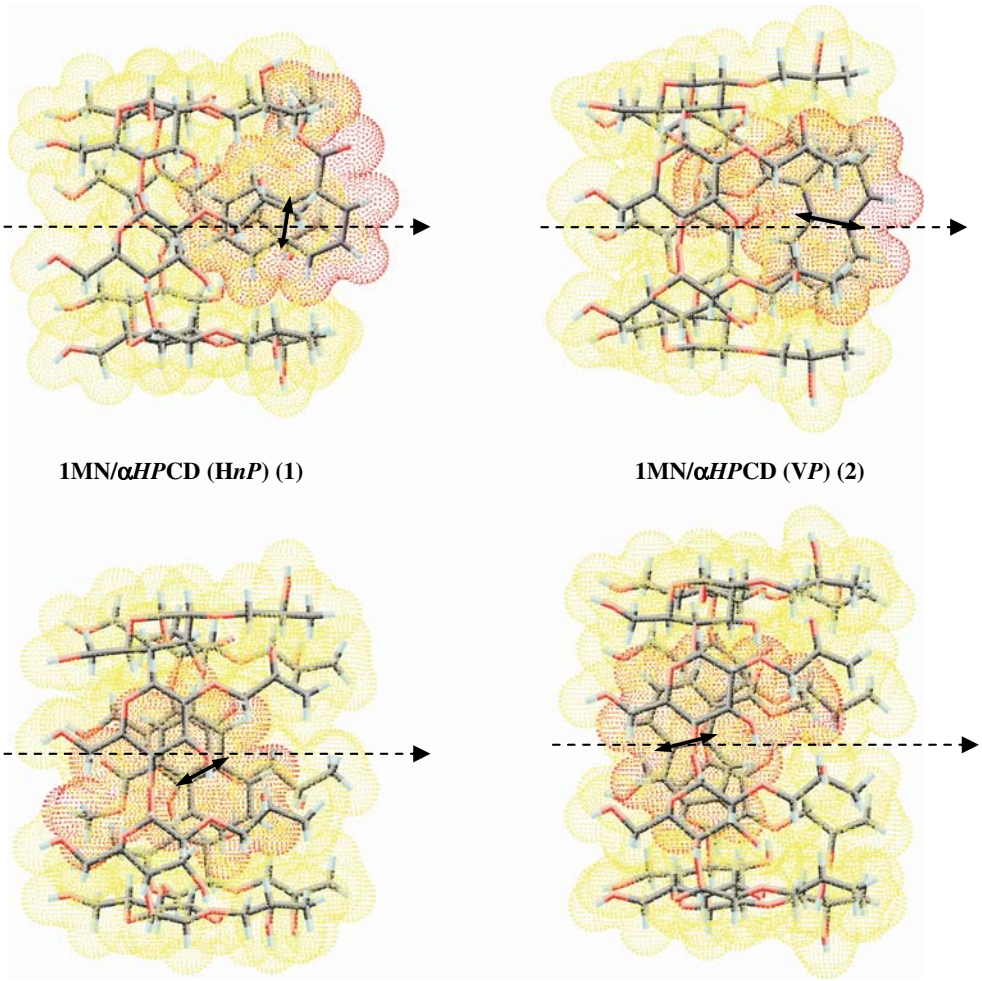


**Fig. 11** Some MBE structures for the 1MN complexes with α*HP*CD (1 and 2), β*HP*CD (3) and γ*HP*CD (4) obtained from representation depicted in Fig. 10

1MN/α*HP*CD H*nP* and V*P* respectively; $y$=1.8 Å; $E_{MBE}$= −63.5 kJmol$^{-1}$ (δ=10.4°) and $y$=−0.72 Å; $E_{MBE}$=−62.4 kJmol$^{-1}$ (δ=11.2°) for 1MN/β*HP*CD (V*P*) and 1MN/γ*HP*CD (V*nP*) complexes respectively. Vertical 1MN oriented structures for these complexes (2, 3 and 4), with δ (short naphthalene axis and the *n*-fold rotation CD axis angle) relatively near zero, may agree with the positive sign of *ICD*. The *ICD* intensity increase may be related with the penetration depth of the 1MN guest ($y$ coordinate) or its relative orientation (value of δ) inside the *HP*CD.

These structures do not disagree with the trend observed in $r_\infty$ values, taking into consideration the possibility of certain movement of 1MN inside the largest size *HP*CD cavities. They may also agree with the results of the quenching experiments and the changes of thermodynamics parameters upon complexation.

Most of the $E_{binding}$ at the MBE is due to non-bonded van der Waals interactions. Electrostatics represents a low percentage of the total binding energy. The total potential energy for 1MN/*HP*CD systems slightly decreases with complexation. The van der Waals interactions are responsible for this decrease. However, they do not represent the largest contributions to the total potential energy of the system. The strain energy, correlated to the *HP*CD cavity size, is the main contribution to the total energy. The latter energy drastically increases for 1MN/α*HP*CD complexation, only slightly for βHPCD and a little for γ*HP*CD. The electrostatics interactions hardly change upon complexation.

## Conclusions

The binding constants for the (1:1) 1MN:*HP*CD complexes are lower compared to the ones obtained with the less bulky 2MN isomer, which is able to penetrate more deeply into the cavities, but they are always larger than when 1MN complexes with the natural un-substituted CDs. Complexation of 1MN with *HP*CDs is accompanied by a less favorable $\Delta H^0$ than that obtained with their natural counterparts. These enthalpy changes agree with the fact

that the van der Waals interactions are mainly responsible for the 1MN/*HP*CD complexation. $\Delta S^0$ may mainly be attributed to the loss of the ordered water around the guest and host cavity upon complexation. This could account for the different penetration and location of the 1MN guest in the complexes. *ICD* spectra, anisotropies at [HPCD]→∞ and bimolecular quenching constants also agree with the MM proposed structures for these complexes.

**Acknowledgements** This research was supported by Comunidad de Madrid (CAM S-055/MAT/0227), Ministerio de Educacion (CTQ2005-04710/BQU) and Consejería de Educación y Ciencia de la Junta de Castilla-La Mancha (grant to M.J.G-A). We wish to express our thanks to M.L. Heijnen for assistance with the preparation of the manuscript.

## References

1. Szejtli J, Osa T (1996) Comprehensive supramolecular chemistry, vol. 3, Cyclodextrins. Elsevier, Oxford
2. D'Souza VT, Lipkowitz KB (eds) (1998) Cyclodextrins. Chem Rev 98(5):1741–2076. doi:10.1021/cr980027p
3. Harada A (2001) Cyclodextrin-based molecular machines. Acc Chem Res 34:456–464. doi:10.1021/ar000174l
4. Nepogodiev SA, Stoddart JF (1998) Cyclodextrin-based catenanes and rotaxanes. Chem Rev 98(5):1959–1976. doi:10.1021/cr970049w
5. Flamigni L (1993) Inclusion of fluorescein and halogenated derivatives in α-, β-, and γ-cyclodextrins: a steady-state and picosecond time-resolved study. J Phys Chem 97(38):9566–9572. doi:10.1021/j100140a006
6. Fraiji EK Jr., Cregan TR, Werner TC (1994) Binding of 2-acetylnaphthalene to cyclodextrins studied by fluorescence quenching. Appl Spectrosc 48(1):79–84. doi:10.1366/0003702944027624
7. Nakamura A, Sato S, Hamasaki K, Ueno A, Toda F (1995) Association of 1:1 inclusion complexes of cyclodextrins into homo- and heterodimers: a spectroscopic study using a TICT-forming fluorescent probe as a guest compound. J Phys Chem 99 (27):10959–10959. doi:10.1021/j100027a040
8. van Stam J, De Feyter S, De Schryver FC, Evans CH (1996) 2-Naphthol complexation by β-cyclodextrin: influence of added short linear alcohols. J Phys Chem 100(51):19959–1996. doi:10.1021/jp961575e
9. Hamai S (1997) Inclusion of 2-chloronaphthalene by α-Cyclodextrin and room-temperature phosphorescence of 2-chloronaphthalene in aqueous D-glucose solutions containing α-cyclodextrin. J Phys Chem B 101(9):1707–1712. doi:10.1021/jp963197j
10. Madrid JM, Villafruela M, Serrano R, Mendicuti F (1999) Experimental thermodynamics and molecular mechanics calculations of inclusion complexes of 9-methyl anthracenoate and 1-methyl pyrenoate with β-cyclodextrin. J Phys Chem B 103 (23):4847–4853. doi:10.1021/jp9838240
11. Sadlej-Sosnowska N, Siemiarczuk A (2001) A time resolved and steady-state fluorescence quenching study on naproxen and its cyclodextrin complexes in water. J Photochem Photobiol Chem 138:35–40. doi:10.1016/S1010-6030(00)00375-0
12. Di Marino A, Mendicuti F (2004) Thermodynamics of complexation of dimethyl esters of tere-, iso-, and phthalic acids with α- and β -cyclodextrins. Appl Spectrosc 58(7):823–830. doi:10.1366/0003702041389283
13. Shannigrahi M, Bagchi S (2005) Time resolved fluorescence study of ketocyanine dye-β cyclodextrin interactions in aqueous and non-aqueous media. Chem Phys Lett 403(1–3):55–61. doi:10.1016/j.cplett.2004.12.098
14. Turro NJ, Okubo T, Weed GC (1982) Enhancement of intramolecular excimer formation of 1,3-bichromophoric propanes via application of high pressure and via complexation with cyclodextrins. Protection from oxygen quenching. Photochem Photobiol 35(3):325–329
15. Kano K, Takenoshita I, Ogawa T (1982) γ -Cyclodextrin-enhanced excimer fluorescence of pyrene and effect of n-butyl alcohol. Chem Lett Chem Soc Jpn 3:321–324
16. Hamai S (1989) Pyrene excimer formation in γ-cyclodextrin solutions: association of 1:1 pyrene-γ -cyclodextrin inclusion compounds. J Phys Chem 93(17):6527–6529. doi:10.1021/j100354a048
17. Pistolis G (1999) Dual excimer emission of p-terphenyl induced by γ-cyclodextrin in aqueous solutions. Chem Phys Lett 304 (5,6):371–377
18. Sainz-Rozas PR, Isasi JR, González-Gaitano G (2005) Spectral and photophysical properties of 2-dibenzofuranol and its inclusion complexes with cyclodextrins. J Photochem Photobiol Chem 173 (3):319–327. doi:10.1016/j.jphotochem.2005.04.011
19. Catena GC, Bright FV (1989) Thermodynamic study on the effects of β-cyclodextrin inclusion with anilinonaphthalenesulfonates. Anal Chem 61(8):905–909. doi:10.1021/ac00183a024
20. Madrid JM, Mendicuti F, Mattice WL (1998) Inclusion complexes of 2-methylnaphthoate and γ-cyclodextrin: experimental thermodynamics and molecular mechanics calculations. J Phys Chem B 102(11):2037–2044. doi:10.1021/jp9728870
21. Di Marino A, Mendicuti F (2002) Fluorescence of the complexes of 2-methylnaphthoate and 2-hydroxypropyl-α -, -β -, and -γ-cyclodextrins in aqueous solution. Appl Spectrosc 56(12):1579–1587. doi:10.1366/000370202321115841
22. Pastor I, Di Marino A, Mendicuti F (2002) Thermodynamics and molecular mechanics studies on α-and β -cyclodextrins complexation and diethyl 2,6-naphthalenedicarboxylate guest in aqueous medium. J Phys Chem B 106(8):1995–2003. doi:10.1021/jp013118q
23. Muñoz de la Peña A, Ndou TT, Zung JB, Warner IM (1991) Stoichiometry and formation constants of pyrene inclusion complexes with β- and γ-cyclodextrin. J Phys Chem 95 (8):3330–3334. doi:10.1021/j100161a067
24. Will AY, Muñoz de la Peña A, Ndou TT, Warner IM (1993) Spectroscopic studies of the interaction of tert-butylamine and n-propylamine with the β-cyclodextrin-pyrene complex. Appl Spectrosc 47(3):277–282. doi:10.1366/0003702934066749
25. Madrid JM, Mendicuti F (1997) Thermodynamic parameters of the inclusion complexes of 2-methylnaphthoate and α- and β-cyclodextrins. Appl Spectrosc 51(11):1621–1627. doi:10.1366/0003702971939604
26. Cervero M, Di Marino A, Mendicuti F (2000) Inclusion complexes of dimethyl 2,6-naphthalenedicarboxylate with α- and β-cyclodextrins in aqueous medium: thermodynamics and molecular mechanics studies. J Phys Chem B 104(7):1572–1580. doi:10.1021/jp993418w
27. Pastor I, Di Marino A, Mendicuti F (2005) Complexes of dihexyl 2,6-naphthalenedicarboxylate with α- and β-cyclodextrins: fluorescence and molecular modelling. J Photochem Photobiol Chem 173(3):238–247. doi:10.1016/j.jphotochem.2005.04.003
28. Alvariza C, Usero R, Mendicuti F (2007) Binding of dimethyl 2,3-naphthalenedicarboxylate with α-, β- and γ-cyclodextrins in aqueous solution. Spectrochem. Acta Part A 67(2):420–429. doi:10.1016/j.saa.2006.07.039
29. Di Marino A, Rubio L, Mendicuti F (2007) Fluorescence and molecular mechanics of 1-methyl naphthalenecarboxylate/cyclo-

dextrin complexes in aqueous medium. J Incl Phenom Macrocycl Chem 58:103–114. doi:10.1007/s10847-006-9129-7
30. Nelson G, Patonay G, Warner IM (1987) Fluorescence lifetime study of cyclodextrin complexes of substituted naphthalenes. Appl Spectrosc 41(7):1235–1238. doi:10.1366/0003702874447617
31. Ferreira JAB, Costa SMB (2005) Non-radiative decay in rhodamines: role of 1:1 and 1:2 molecular complexation with β-cyclodextrin. J Photochem Photobiol Chem 173(3):309–318. doi:10.1016/j.jphotochem.2005.04.010
32. Serna L, Di Marino A, Mendicuti F (2005) Inclusion complexes of a bichromophoric diester containing anthracene and naphthalene groups with alpha- and beta-cyclodextrins: thermodynamics and molecular mechanics. Spectrochim Acta Part A Mol Biomol Spectrosc 61(8):1945–1954. doi:10.1016/j.saa.2004.07.033
33. Hossain MA, Mihara H, Ueno A (2003) Fluorescence resonance energy transfer in a novel cyclodextrin-peptide conjugate for detecting steroid molecules. Bioorg Med Chem Lett 13(24):4305–4308. doi:10.1016/j.bmcl.2003.09.051
34. Park JW, Lee SY, Kim SM (2005) Efficient inclusion complexation and intra-complex excitation energy transfer between aromatic group-modified β-cyclodextrins and a hemicyanine dye. J Photochem Photobiol Chem 173(3):271–278. doi:10.1016/j.jphotochem.2005.04.006
35. Nigam S, Durocher G (1997) Inclusion complexes of some 3H-indoles with cyclodextrins studied through excited state dynamics and steady state absorption and fluorescence spectroscopy. J Photochem Photobiol A: Chem 103(1,2):143–152
36. Lipkowitz KB (1998) Applications of computational chemistry to the study of cyclodextrins. Chem Rev 98(5):1829–1873. doi:10.1021/cr9700179
37. Jursic BS, Zdravkovski Z, French AD (1996) Molecular modeling methodology of β-cyclodextrin inclusion complexes. J Mol Struct Theochem 366(1–2):113–117. doi:10.1016/0166-1280(96)04521-6
38. Salvatierra D, Jaime C, Virgili A, Sanchez-Ferrando F (1996) Determination of the inclusion geometry for the β -cyclodextrin/benzoic acid complex by NMR and molecular modeling. J Org Chem 61(26):9578–9581. doi:10.1021/jo9612032
39. Madrid JM, Pozuelo J, Mendicuti F, Mattice WL (1997) Molecular mechanics study of the inclusion complexes of 2-methyl naphthoate with α- and β-cyclodextrins. J Colloid Interface Sci 193(1):112–120. doi:10.1006/jcis.1997.5061
40. Pozuelo J, Nakamura A, Mendicuti F (1999) Molecular mechanics study of the complexes of β-cyclodextrin with 4-(dimethylamino) benzonitrile and benzonitrile. J Incl Phenom Macrocycl Chem 35 (3):467–485. doi:10.1023/A:1008018502072
41. Cervello E, Mazzucchi F, Jaime C (2000) Molecular mechanics and molecular dynamics calculations of the β -cyclodextrin inclusion complexes with m-, and p-nitrophenyl alkanoates. J Mol Struct (Theochem) 530(1,2):155–163
42. Lino ACC, Takahata Y, Jaime C (2002) α-and β -cyclodextrin complexes with n-alkyl carboxylic acids and n-alkyl p-hydroxy benzoates. A molecular mechanics study of 1:1 and 1:2 associations. J Mol Struct Theochem 594(3):207–213. doi:10.1016/S0166-1280(02)00393-7
43. Di Marino A, Mendicuti F (2007) Rationalizing some experimental facts on the complexation of 2-methyl naphthalenecarboxylate and hydroxypropyled cyclodextrins by molecular mechanics and molecular dynamics. J Incl Phenom Macrocycl Chem 58(3–4):295–305. doi:10.1007/s10847-006-9157-3
44. Pozuelo J, Mendicuti F, Mattice WL (1997) Inclusion complexes of chain molecules with cycloamyloses. 2. molecular dynamics simulations of polyrotaxanes formed by poly(ethylene glycol) and α-cyclodextrins. Macromolecules 30(12):3685–3690. doi:10.1021/ma961270y
45. Lipkowitz KB, Pearl G, Coner B, Peterson MA (1997) Explanation of where and how enantioselective binding takes place on permethylated β-cyclodextrin, a chiral stationary phase used in gas chromatography. J Am Chem Soc 119(3):600–610. doi:10.1021/ja963076x
46. Köhler J, Hohla M, Söllner R, Eberle H-J (1998) Cyclohexadecanone derivative/γ-cyclodextrin complexes MD simulations and AMSOL calculations in vacuo and in aquo compared with experimental finding. Supramol Sci 5(1–2):101–116. doi:10.1016/S0968-5677(97)00065-5
47. Pozuelo J, Mendicuti F, Mattice WL (1998) Inclusion complexes of chain molecules with cycloamylosesIII. Molecular dynamics simulations of polyrotaxanes formed by polypropylene glycol and β -cyclodextrins. Polym J 30(6):479–484. doi:10.1295/polymj.30.479
48. Dodziuk H, Kozminski W, Lukin O, Sybilska D (2000) NMR manifestations and molecular dynamics modeling of chiral recognition of α-pinenes by α-cyclodextrin. J Mol Struct Theochem 525:205–212
49. Grabuleda X, Ivanov P, Jaime C (2003) Computational studies on pseudorotaxanes by molecular dynamics and free energy perturbation simulations. J Org Chem 68(4):1539–1547. doi:10.1021/jo0265636
50. Krois D, Brinker UH (2006) In: Dodziuk H (ed) Cyclodextrins and their complexes, Chapter 10.4. Wiley-VCH, pp 289–298
51. Murphy RS, Barros TC, Mayer B, Marconi G, Bohne C (2000) Photophysical and theoretical studies on the stereoselective complexation of naphthylethanols with β-cyclodextrin. Langmuir 16(23):8780–8788. doi:10.1021/la0005311
52. Mendicuti F, Patel B, Mattice WL (1990) Intramolecular formation of excimers in model compounds for polyesters containing naphthalene units: α,ω-diesters from 1-naphthoic acid and five glycols. Polymer (Guildf) 31(10):1877–1882. doi:10.1016/0032-3861(90)90010-V
53. O'Connor DV, Ware WR, Andre JC (1979) Deconvolution of fluorescence decay curves. A critical comparison of techniques. J Phys Chem 83:1333–1343. doi:10.1021/j100473a019
54. Lakowicz JR (1999) Principles of fluorescence spectroscopy, 2nd edn. Kluwer, New York, p 129
55. Lakowicz JR (1999) Principles of fluorescence spectroscopy, 2nd edn. Kluwer, New York, p 298
56. Valeur B (2002) Molecular fluorescence: principles and applications. Wiley-VCH, Weinheim, p 89
57. Mendicuti F (2006) Application of fluorescence techniques and modelling to the study of the complexation of chromophore-containing guests with cyclodextrins. Trends Phys Chem II, 61–77
58. Sybyl 6.9; Tripos Associates; St. Louis, Missouri, USA
59. Clark M, Cramer RC III, Van Opdenbosch N (1989) Validation of the general purpose Tripos 5.2 force field. J Comput Chem 10 (8):982–1012. doi:10.1002/jcc.540100804
60. MOPAC (AM1). Included in the Sybyl package
61. Usero R, Alvariza C, González-Álvarez MJ, Mendicuti F (2008) Complexation of dimethyl 2,3-naphthalenedicarboxylate with 2-hydroxypropyl-α-, -β- and -γ-cyclodextrins in aqueous solution by fluorescence, circular dichroism and molecular mechanics. J Fluoresc (in press)
62. Job P (1928) Formation and stability of inorganic complexes in solution. Ann Chim 9:113–203
63. Loukas YL (1997) Multiple complex formation of fluorescent compounds with cyclodextrins: efficient determination and evaluation of the binding constant with improved fluorometric studies. J Phys Chem B 101:4863–4866. doi:10.1021/jp9638189
64. Platt JR (1949) Classification of spectra of cata-condensed hydrocarbons. J Chem Phys 17:484–495. doi:10.1063/1.1747293

65. Kodaka M (1998) Application of a general rule to induced circular dichroism of naphthalene derivatives complexed with cyclodextrins. J Phys Chem 102(42):8101–8103
66. Yorozu T, Hoshino M, Imamura M (1982) Fluorescence studies of pyrene inclusion complexes with α-, β-, and γ-cyclodextrins in aqueous solutionsEvidence for formation of pyrene dimer in γ -cyclodextrin cavity. J Phys Chem 86(22):4426–4429. doi:10.1021/j100219a031
67. Kodaka M (1991) Sign of circular dichroism induced by β -cyclodextrin. J Phys Chem 95(6):2110–2112. doi:10.1021/j100159a005
68. Kodaka M (1993) A general rule for circular dichroism induced by a chiral macrocycle. J Am Chem Soc 115(9):3702–3705. doi:10.1021/ja00062a040
69. Neckers DC, Volman DH, VonBünau G (1996) Advances in photochemistry. Wiley, New York, pp 5–35